



Antioxidative study of Cerium Oxide nanoparticle functionalised PCL-Gelatin electrospun fibers for wound healing application



Hilal Ahmad Rather^a, Ria Thakore^b, Ragini Singh^b, Dhvani Jhala^a, Sanjay Singh^b, Rajesh Vasita^{a,*}

^a Biomaterials & Biomimetics Laboratory, School of Life Sciences, Central University of Gujarat, Gandhinagar, 382030, Gujarat, India

^b Division of Biological and Life Sciences, School of Arts and Science, Ahmedabad University, Navrangpura, Ahmedabad, 380009, Gujarat, India

ARTICLE INFO

Article history:

Received 9 August 2017

Received in revised form

25 September 2017

Accepted 26 September 2017

Available online 2 October 2017

Keywords:

Electrospinning

Ce nanoparticles

Antioxidative

Nanofiber

ABSTRACT

Skin wound healing involves a coordinated cellular response to achieve complete reepithelialisation. Elevated levels of reactive oxygen species (ROS) in the wound environment often pose a hindrance in wound healing resulting in impaired wound healing process. Cerium oxide nanoparticles (CeNPs) have the ability to protect the cells from oxidative damage by actively scavenging the ROS. Furthermore, matrices like nanofibers have also been explored for enhancing wound healing. In the current study CeNP functionalised polycaprolactone (PCL)-gelatin nanofiber (PGNPNF) mesh was fabricated by electrospinning and evaluated for its antioxidative potential. Wide angle XRD analysis of randomly oriented nanofibers revealed ~2.6 times reduced crystallinity than pristine PCL which aided in rapid degradation of nanofibers and release of CeNP. However, bioactive composite made between nanoparticles and PCL-gelatin maintained the fibrous morphology of PGNPNF upto 14 days. The PGNPNF mesh exhibited a superoxide dismutase (SOD) mimetic activity due to the incorporated CeNPs. The PGNPNF mesh enhanced proliferation of 3T3-L1 cells by ~48% as confirmed by alamar blue assay and SEM micrographs of cells grown on the nanofibrous mesh. Furthermore, the PGNPNF mesh scavenged ROS, which was measured by relative DCF intensity and fluorescence microscopy; and subsequently increased the viability and proliferation of cells by three folds as it alleviated the oxidative stress. Overall, the results of this study suggest the potential of CeNP functionalised PCL-gelatin nanofibrous mesh for wound healing applications.

© 2017 The Authors. Production and hosting by Elsevier B.V. on behalf of KeAi Communications Co., Ltd. This is an open access article under the CC BY-NC-ND license (<http://creativecommons.org/licenses/by-nc-nd/4.0/>).

1. Introduction

Reactive oxygen species (ROS) are critical players of the wound healing process. Low levels of ROS play physiological role in normal wound healing, notably act as cellular messengers to stimulate cell migration, inflammation and angiogenesis associated with wound healing. In the inflammatory phase, neutrophils and macrophages arrive at a wound lesion and secrete large amounts of ROS along with pro-inflammatory cytokines [1]. The ROS directly attack invading pathogens, kill them and aid their phagocytosis [2]. Furthermore, moderate levels of ROS accelerates angiogenesis by upregulating the production of the vascular endothelial growth

factor in keratinocytes [3,4]. ROS are also involved in re-epithelialization. They trigger the activation of epidermal growth factor receptors and the keratinocyte growth factor receptors [5,6] and induces the production of TGF- α in fibroblasts. Hence, ROS can support the migration and proliferation of epidermal cells and therefore enhance wound healing. However, uncontrolled production of ROS produces superoxides which damages the tissue by reduction in antioxidant production and activity [7]. In early stages, wounds with impaired healing have elevated levels of ROS, however, the activity of anti-oxidant enzymes are not elevated, which leads to increased oxidative stress in the wound environment [8]. The early generation of ROS in presence of nicotinamideadenine-dinucleotide-dependent oxidases that are produced by resident endothelial cells and fibroblasts causes impaired wound healing [9]. According to Rodriguez et al., both hypoxia and hyperoxia increases ROS levels which transcends the beneficial effect and

* Corresponding author.

E-mail address: rajesh.vasita@cug.ac.in (R. Vasita).

Peer review under responsibility of KeAi Communications Co., Ltd.

causes additional tissue damage [10]. Furthermore, elevated ROS in the wound environment have decelerating effects on angiogenesis and lead to a stagnant inflammatory phase, which further damages tissue through excessive production or activation of reactive oxygen intermediates, inflammatory cytokines, proteases, proapoptotic proteins causing increased cell death [11] that lead to wounds with impaired healing [12,13]. Therefore, controlling the levels of ROS at the wound environment may be a viable option to enhance the wound healing.

Different nanoparticle based approaches for decreasing the ROS levels have been used to enhance wound healing [14–16]. Recently, cerium oxide nanoparticles (CeNP) have gained attention for applications in wound healing. This is because CeNPs have a capacity to alternate between two oxidation states: 3^+ and 4^+ due to an oxygen vacancy in their crystal structure [17]. Due to this autoregenerative cycle, they can be used as antioxidant agents [18–20]. Their ROS scavenging ability alleviates the oxidative stress experienced by cells in the wound environment [14,15,21,22].

Electrospun nanofibers have been widely used for skin tissue engineering applications due to their ECM mimicking property, biodegradability and biocompatibility [23]. Blended natural and synthetic biomaterials including PCL-gelatin [23], polyurethane-gelatin (28), poly(L-lactic acid)-*b*-poly(*ε*-caprolactone)-gelatin [24], PCL-collagen [25], poly(lactic-*co*-glycolic acid)-collagen [26], were extensively explored for skin tissue engineering applications. Blending combines the biological properties of natural polymers and the physicochemical properties synthetic polymers [27,28]. Nanofibers can also be functionalised with certain agents like drugs [29], growth factors [30] and nanoparticles [31] that enhance the wound healing mechanism. Nanofibers incorporated with nanoparticles like silver [32–35], zinc oxide, chitosan [36], gold [37–39] have been assessed for wound healing applications. In a study using spirulina extract derived from blue-green algae as an antioxidant and anti-inflammatory agent. Spirulina extract-loaded PCL nanofiber wound dressings have been found to increase the fibroblast viability *in vitro* by suppressing the function of ROS. *In vivo* assays carried out using these nanofibers have showed increased rate of wound healing and skin regeneration [40].

Therefore, in current study PCL-Gelatin nanofibers have been fabricated as a reservoir of CeNPs to reduce the ROS levels produced by the oxidative stress of mouse fibroblasts. The CeNPs loaded nanofibers were characterized for their degradation behaviour and crystallinity. At multiple time points released nanoparticles were used for superoxide dismutase (SOD) mimetic activity. For biological characterisation direct contact assay (cells were grown on CeNPs loaded nanofiber) and indirect assay (leached nanoparticles was included in cell culture medium) were performed with 3T3L1 mouse fibroblast cells.

2. Materials and methods

2.1. Materials

Polycaprolactone (PCL) (average M_n 80 kDa), gelatin powder (type A from porcine skin), cerium nitrate hexahydrate ($Ce(N-O_3)_3 \cdot 6H_2O$), ferricytochrome C, xanthine oxidase, resazurin sodium salt, poly(2-hydroxyethyl methacrylate) (polyHEMA) and 2,7-dichlorofluorescein diacetate (DCFDA) were purchased from Sigma Aldrich (USA). 1,1,1,3,3,3-Hexafluoro-2-propanol (HFIP), 99% was obtained from Alfa Aesar (India). Dulbecco's modified eagle's media-high glucose (DMEM-HG) and fetal bovine serum (FBS) were obtained from Gibco (India). Hypoxanthine was purchased from Hi-Media Pvt. Ltd. (India). Hydrogen peroxide 30%w/v (H_2O_2) was purchased from Nice Chemicals Pvt. Ltd. (India). 3T3-L1 cell line

was obtained from National Centre for Cell Sciences (NCCS) (Pune, India).

2.2. Synthesis of nanoparticles

Cerium nitrate hexahydrate was used for synthesis of cerium oxide nanoparticles (5 mM, 30 mM) using previously published method [41]. Briefly, specific quantity of cerium nitrate hexahydrate was dissolved in 49 mL of deionized water and 1 mL hydrogen peroxide was added. The solution was then aged at room temperature for 10–15 days in order to obtain nanoceria with a high $3^+/4^+$ state. This transition was also signified by conversion of color of solution from yellow to colorless.

2.3. Dynamic light scattering (DLS)

Zeta potential of CeNPs was measured by using dynamic light scattering measurements from Zeta Sizer Nano (Malvern Instruments, United Kingdom) which uses a laser with wavelength of 633 nm.

2.4. Transmission electron microscopy (TEM)

Sample was prepared by adding drop of CeNPs on carbon coated copper grid. After drying the images of CeNPs were acquired by using transmission electron microscope JEOL 2010-F TEM, Japan.

2.5. Fabrication of PCL-Gelatin nanofibers loaded with cerium oxide nanoparticles (CeNPs)

A polymer solution of PCL-Gelatin was prepared by mixing 10% w/v PCL and 20% w/v gelatin in HFIP solvent system for 6–12 h. For CeNP loaded nanofibers (PGNPNF), a 25% v/v 30 mM CeNP solution was added to the polymer solution; whereas for control samples nanoparticle solution was replaced with similar amount of distilled water. Both samples were electrospun using E-spin Nanotech, India electrospinning unit. Briefly, the polymer solution was filled in a 5 mL BD syringe fitted with a 26 gauge blunt end needle. The polymer solution was oozed out at a continuous flow rate of 1 mL/h using a syringe pump. A fixed electrical potential of 1 kV/cm was applied across a distance of 15 cm between the tip of the needle and the collector. The resulting electrospun nanofibers were collected on aluminium foil and glass coverslips (18 × 18 mm) for characterisation and cell culture studies, respectively.

2.6. Scanning electron microscopy

The morphological study of the nanofibers was performed using scanning electron microscopy (SEM) (EVO 18, Zeiss, Germany). After fabrication, the nanofibers were lyophilized and then sputter coated with gold-palladium followed by SEM imaging. The diameters of the PGNF and PGNPNF were determined by measuring randomly selecting 50 fibers from each, using ImageJ software (National Institute of Health, USA).

2.7. Fourier transform infrared spectroscopy

The chemical characterisation of nanofibers was performed using attenuated total reflection Fourier transform infrared spectroscopy (ATR-FTIR) (Agilent, USA). FTIR spectra of PGNF, PGNPNF, gelatin powder and PCL film were recorded in a range of 400–4000 cm^{-1} with a resolution of 4 cm^{-1} at data intervals of 1 cm^{-1} . Multiple spectra were recorded for each nanofiber sample by taking sections from different areas of the sample.

2.8. Wide angle X-Ray diffraction

X-ray diffraction analysis was performed to detect changes at the crystal structure level of polymers used for nanofiber fabrication. Analysis was done using a wide angle X-ray diffractometer (XRD) (D8 discover, Bruker, USA). X-rays were generated at 40 kV and 30 mA and the goniometer was rotated from 5° to 50° at the rate of 0.05° increment per step with 0.2 s per step speed. A thin film setup was used for PGNF, PGPNPF and PCL film with a grazing angle of 2°. The measurements were recorded at an ambient temperature.

2.9. Degradation study

The degradation behaviour of PGNF and PGPNPF was studied to ensure their integrity in biological conditions. Nanofibers meshes were cut into 1 cm × 1 cm pieces and immersed in centrifuge tubes containing sterile PBS. The tubes were placed in a shaking water bath at 37 °C and 40 RPM for a duration of 14 days. The PBS was changed every 3–4 days to maintain the ionic conditions. At each predetermined time point, a centrifuge tube containing the PGNF and PGPNPF nanofiber samples were taken out of the water bath. The nanofibers were desiccated for 1–2 h followed by lyophilisation for 24 h and then stored at –20 °C before use. The degraded samples were analysed using SEM.

2.10. Superoxide dismutase (SOD) enzyme mimetic activity measurement

For SOD mimetic study, 48 mg of PGNF and PGPNPF were weighed and incubated in 500 µl of Tris buffer and PBS for different time period (30 min, 24, 48 and 96 h). Released CeNPs in respective buffer were considered to evaluate the SOD mimetic activity. A volume of 40 µl buffer was used for reaction and equal amount of fresh buffer was added to maintain the releasing medium volume constant. SOD mimetic activity was measured, as described previously by Korsvik et al. [19]. In brief, reduction of ferri-cytochrome C by superoxide were monitored spectrophotometrically at 550 nm for 20 min. In the reaction hypoxanthine/xanthine oxidase system was used for generation of superoxide radicals and catalase were added to degrade hydrogen peroxide produced as a side reaction. Total reaction volume was maintained as 100 µl as performed in 96 well plate.

2.11. Cell culture studies

Mouse embryo fibroblasts 3T3-L1 cells were cultured in DMEM-HG medium supplemented with 10% FBS and 1% antibiotic antimycotic solution mixture. The cells were incubated at 37 °C and 5% CO₂ and subcultured at about 70% confluency. For cell culture studies, nanofibers deposited on glass coverslips were sterilised under UV light for 60 min each on both sides. 50,000 cells were seeded on each nanofiber sample and were allowed to adhere to the nanofibers for 1–2 h, followed by more media being added gradually.

2.12. Cell proliferation assay

The viability and proliferation of 3T3-L1 cells on nanofibers was assessed by alamar blue assay over a period of 72 h. The viable cells convert resazurin, a non-fluorescent compound to a fluorescent red compound resorforin that can be quantified spectrophotometrically and is directly proportional to the number of living cells. After every 24 h, cells were incubated with alamar blue solution (0.15 mg/mL in PBS, pH = 7.4) at 10% volume of the cell culture

medium for 1 h; then the absorbance was measured at 570 nm using a multiplate reader (Synergy H1, Biotek Instruments, USA). A graph of absorbance versus the number of days was plotted using GraphPad Prism 5 software (USA).

2.13. Cell morphological studies

The morphology of cells grown on nanofibers was analysed by SEM, 24 h post seeding. For SEM, the cells on nanofibers were washed with PBS and fixed with 2% glutaraldehyde in 0.1 M sodium cacodylate buffer (pH = 7.2) for 1 h and were transferred to 0.1 M cacodylate buffer. Following this, a gradient dehydration was carried out by washing cells with 30%, 70%, 80%, 90%, 95% and absolute ethanol for 5–10 min each. The nanofiber samples were then desiccated for 2 h and lyophilized for 24 h. The samples were then sputter coated with gold-palladium and observed under SEM.

2.14. In vitro antioxidant study

In this study, the antioxidant potential of the nanofibers was evaluated by determining their potential to scavenge ROS. DCFDA, a cell permeable fluorogenic probe was used to detect intracellular ROS level. DCFDA can be internalised by cells where in it is deacetylated by cellular esterases to a nonfluorescent compound which can be later oxidised by ROS to a fluorescent compound 2',7'-dichlorofluorescein (DCF) which can be estimated spectrophotometrically. For this study, extracts of PGNF and PGPNPF were used. The extracts were prepared by immersing nanofibers weighing 40 mg in 10 mM Tris (pH = 7.5) for 30 min. Meanwhile 10,000 cells were seeded in 96 well plates. After 24 h, cells were treated with 50 µM H₂O₂ in media for 30 min and then incubated with 20% diluted extract of either PGPNPF or PGNF for 24 h. Meanwhile, some set of wells incubated with Tris were regarded as negative (-ve) control. Afterwards, DCFDA dye (20 µM in 1X PBS) was added to each well and the plate was incubated for 30 min at 37 °C in dark. The fluorescence was measured at excitation and emission wavelength of 480 nm and 530 nm, respectively using Synergy H1, Biotek Instruments, U.S.A.

2.15. Intracellular ROS measurement

The ROS scavenging potential of nanofibers was further studied by fluorescence microscopy. Briefly, 10,000 cells were seeded in 96 well plate. When cells reached up to 75% confluency, they were treated with 50 µM H₂O₂ for 30 min followed by incubation with diluted extract of PGNF and PGPNPF. The extracts were collected after immersing nanofibers in Tris for 30 min and 24 h respectively. Control wells were treated with equal volume of Tris in media. After 24 h of treatment, cells were incubated with DCFDA dye for 30 min. The cells were then washed with PBS and fixed with 2% paraformaldehyde for 30 min. Afterwards, imaging was done under fluorescent microscope (Axio Observer, Zeiss, Germany). The relative fluorescence intensity was calculated from the images of different groups by ImageJ software.

2.16. Cellular protection against ROS

The cytoprotective potential of the nanofibers against the ROS was evaluated by determining the viability of the cells. The viability was evaluated 24 h post treatment of ROS. Briefly, 50,000 cells were seeded directly on PGNF, PGPNPF and TCPS (control). After 24 h, cells were treated with 50 µM H₂O₂ in media for 30 min and then incubated with normal media for next 24 h. Cells were then incubated with alamar blue solution (0.15 mg/mL in PBS, pH = 7.4) at 10% volume of the cell culture medium for 1 h; then the absorbance

was measured at 570 nm using a multiplate reader (Synergy H1, Biotek Instruments, USA). A graph of absorbance versus the number of days was plotted using GraphPad Prism 5 software (USA). For control, cells were grown on TCPS with the assumption that they provide no antioxidant activity.

2.17. Statistical analysis

The results were analysed using GraphPad Prism 5 software (version 5.01). The statistical comparison was carried out using Student's t-test, with a p-value used to indicate significance. (* $p < 0.05$, ** $p < 0.01$, *** $p < 0.001$).

3. Results and discussion

3.1. Nanoparticle characterisations

As, prepared CeNPs were characterized by TEM and DLS. The size and shape of CeNPs were examined by TEM imaging. The nanoparticles were of uniform size and appeared to be quasi spherical in shape Fig. 1(a). Particles were found to be of ~42 nm in size as shown by particle size distribution of TEM image Fig. 1(b). The Zeta potential value of CeNPs suspended in water were recorded as 30.8 mV Fig. 1(c), which depicts that particles are well stable in colloid suspension.

3.2. Fabrication of nanofibers

Nanofibers have been fabricated by electrospinning of PCL and gelatin. Studies have shown that blending of PCL and gelatin overcomes the drawbacks of natural and synthetic polymers, yielding a biomaterial that is biocompatible, has good mechanical, chemical and physical properties and promotes cell adhesion [42]. Furthermore, PCL-gelatin nanofibers have been explored for applications in wound healing and skin regeneration [23,43]. PCL-gelatin nanofibers have also been used as carriers for drugs [44], growth factors [30] as well as nanoparticles [45] and explored for aiding in the wound healing process. CeNPs, have emerged as candidates for enhancing the intrinsic wound healing mechanism due to their antioxidant behaviour. In this study PGNF were fabricated from a polymer solution of 10% w/v PCL, 20% w/v gelatin and

25% v/v distilled water. PGNPNF were fabricated from polymer solutions of 10% w/v PCL and concentration of gelatin varying in the range of 10–20% w/v. Furthermore, two different concentrations of CeNP solution (5 mM and 30 mM) were used to synthesise PGNPNF nanofibers (data not shown). The optimized PGNPNF nanofibers were fabricated from a polymer solution of 10% w/v PCL, 20% w/v gelatin and 25% v/v 30 mM CeNP solution. As PCL is hydrophobic and gelatin is hydrophilic in nature, they have quite dissimilar solubility in different solvents. HFIP is an organic solvent in which both these polymers are soluble and it also serves as a good solvent for electrospinning due to its higher volatility and conductivity. Moreover, use of HFIP as a single solvent allows more miscibility between PCL and gelatin and therefore results in homogenous composition of nanofibers [46].

In addition to polymer concentration and solvent selection, other parameters such as flow rate, distance and voltage were also optimized in order to get bead-free nanofibers. Distance between needle and collector is one of the most crucial parameters that affect nanofiber morphology. To accommodate more number of CeNPs, comparatively thicker nanofibers were required for this study. Furthermore, increase in the distance between needle and collector causes reduction in the electrostatic field strength and hence results in increased fiber diameter [47]. Therefore, after investigating different variables, we finalised 15 cm as the optimum distance for PGNF fabrication, as it allowed proper solvent evaporation as well as continuous bead free fiber formation.

Morphology analysis of PGNF and PGNPNF was carried out by observing the nanofibers using SEM. The SEM micrographs of PGNF and PGNPNF shown in Fig. 2(a and b) reveal isotropic and randomly oriented nanofibers with a seemingly smooth morphology. The diameter of the PGNF nanofibers was calculated to be in the range of 290–650 nm with a mean fiber diameter of 486 ± 110 nm. Whereas, the diameter of the PGNPNF nanofiber was estimated to be in the range of 300–760 nm with a mean fiber diameter of 611 ± 206 nm. Studies have shown that CeNPs are nonconductive in nature [42]. Therefore, a CeNP containing solution may have reduced conductivity and resulted into thicker nanofibers [25].

3.3. FTIR and XRD analysis

The FTIR spectra of PCL shows sharp characteristic peak of

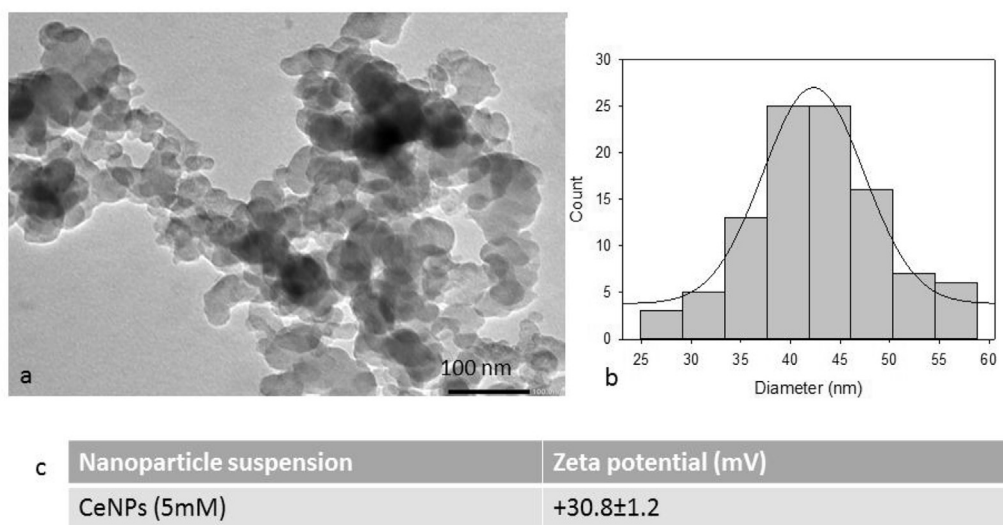


Fig. 1. Characterization of nanoparticles: (a) TEM image of CeNPs, (b) Particle size distribution of CeNPs and (c) Zeta potential of CeNPs using dynamic light scattering.

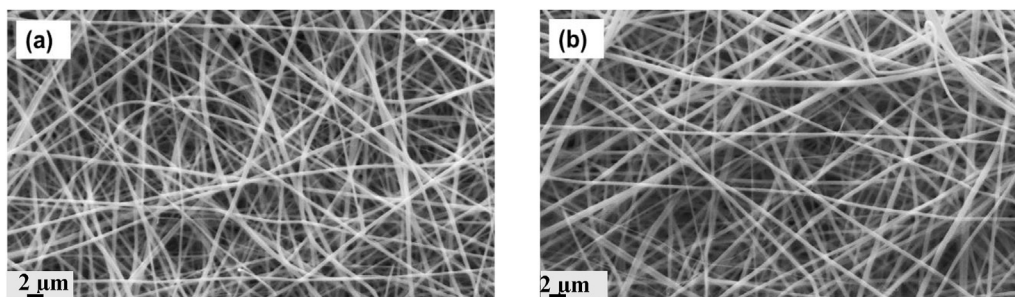


Fig. 2. SEM images of randomly oriented (a) PGNF, (b) PGNPf fabricated by electrospinning.

carbonyl stretching at 1720 cm^{-1} and a smaller peak of asymmetric and symmetric CH_2 stretching at 2943 cm^{-1} and 2865 cm^{-1} respectively Fig. 3(a). While in case of gelatin, distinct peaks of carbonyl stretching of amide-I group and N–H bending of amide-II group were observed at 1640 cm^{-1} and 1540 cm^{-1} respectively. This results confirm the presence of polymer but did not provide any information on possible interaction between two polymers [43,48]. However, the presence of amide and carboxyl groups on nanofibrous surface are advantageous as it supports fibroblast attachment and proliferation [49].

The X-ray diffractogram of PCL, PGNF and PGNPf are shown in Fig. 3(b). Two major sharp peaks were observed in the diffractogram of PCL film at 21.3° and 23.8° that represent (1 1 0) and (2 0 0) planes of a polyethylene like structure, respectively [27]. The PGNF and PGNPf showed a peak characteristic to PCL at the same Bragg's angle of 23.8° , but at a much reduced intensity. Furthermore, crystallinity index i.e. area under curve was calculated from the diffractogram which also shows the reduced crystallinity of PCL in PGNF and PGNPf. The area under curve has reduced from 21,412.05 for PCL film to 5789.65 for PGNF and 8084.475 for PGNPf. These results suggest that blending of PCL and gelatin significantly reduced the crystallinity of PCL in nanofiber. However, incorporation of CeNPs had relatively lesser change in crystallinity. This reduced crystallinity in the nanofiber structure is beneficial as it enhances cell adhesion and biocompatibility [27]. Indeed, decrease in crystallinity will accelerate the PCL degradation which is known to be slow degrading polymer. However, in current study

relatively faster degradation was aimed for rapid release of nanoparticles. Reduction in the crystallinity corresponds with the degradation study, which shows less degradation in PGNPf compared to PGNF.

3.4. Degradation study

The stability of the PGNF and PGNPf meshes in a biological environment was studied by a degradation study up to 14 days. The nanofibrous meshes were allowed to degrade in PBS without any external enzyme. In both cases, the PCL was degraded by hydrolysis of ester linkage and exposed the $-\text{COOH}$ and $-\text{OH}$ on nanofiber surface [50]. The ionization of $-\text{COOH}$ groups increased the hydrophilicity followed by more water uptake leading to degradation and release of nanoparticles. Fig. 4 (a,c,e) shows the degradation profile of the PGNF nanofibers after 1, 4, and 14 days which indicated significant morphological changes. During degradation very few individual fibers were observed while most of the fibers of different layers of the PGNF were fused together to form a continuous non-fibrous mat like structure. A considerable decrease in the fiber diameter was also remarked during the 14 day degradation. The diameter of PGNF decreased to $367 \pm 62\text{ nm}$ from an initial diameter of $486 \pm 110\text{ nm}$ after 14 day degradation period. The significant loss of weight and fibrous nature made sample brittle and difficult to handle. As can be seen from Fig. 4 (b,d,f), the PGNPf meshes demonstrated progressive degradation. The edges of the interconnected nanofibers fused together and did not retain

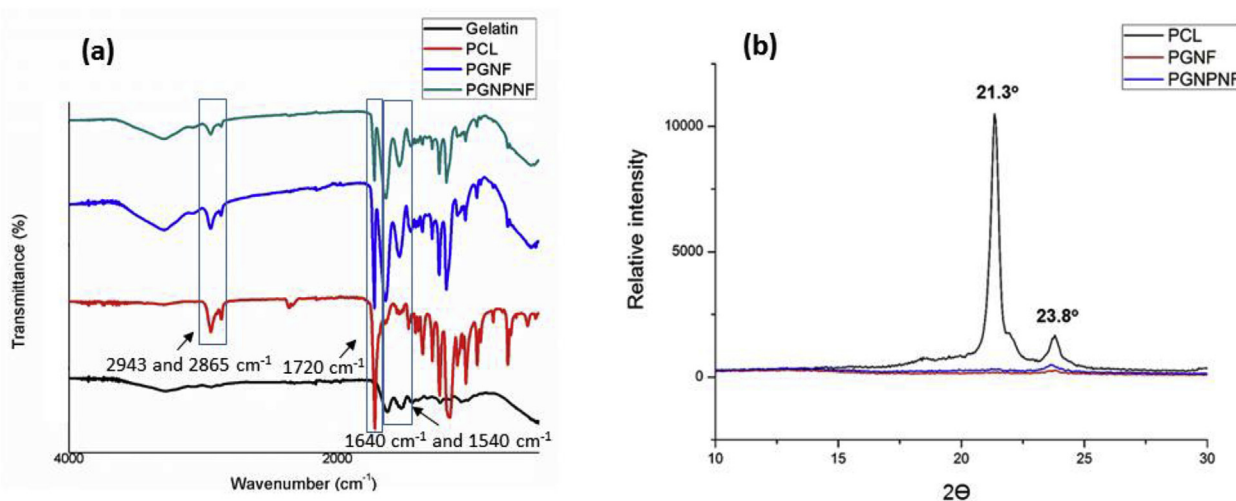


Fig. 3. (a) The FTIR spectra of gelatin powder (black), PCL film (red), PGNF (blue) and PGNPf (green) (b): Wide-angle X-ray diffractogram of PCL film PGNF (red) and PGNPf (blue).

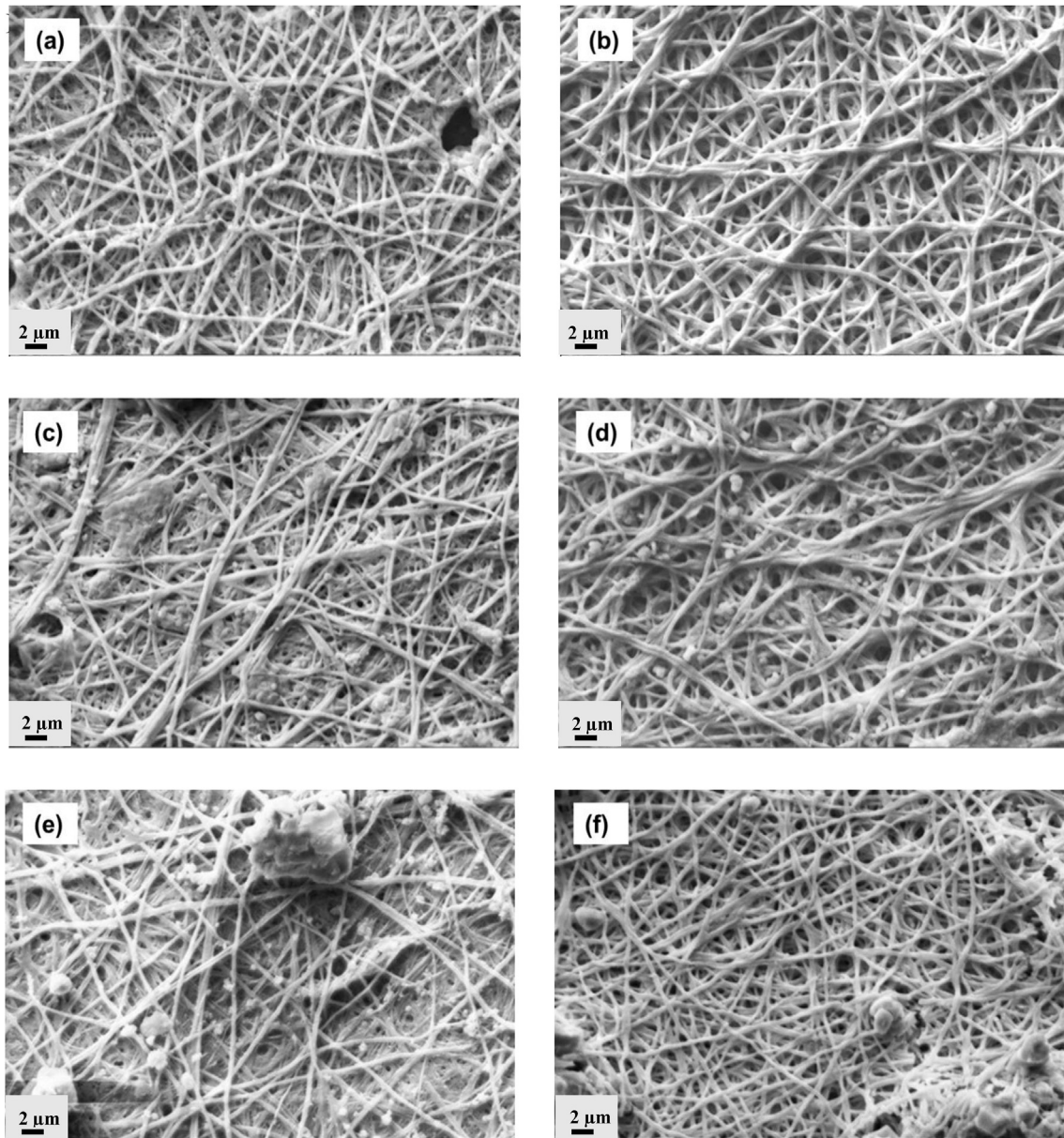


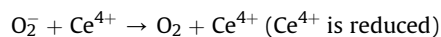
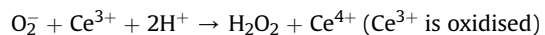
Fig. 4. SEM micrographs of degradation study of PGNF after (a) day 1 (c) day 4 (e) day 14 and of PGNPNF after (b) day 1 (d) day 4 (e) day 14 in phosphate buffer at pH7.2.

the distinct individual nanofiber morphology that was observed before degradation. However, even during degradation the nanofibers still retained fibrous morphology and porous structure which was lacking in case of PGNF meshes. Furthermore, it was also accompanied with a decrease in the diameter from an initial 611 ± 206 nm to 387 ± 73 nm over a period of 14 days. Indeed, the decrease in crystallinity expedited the rate of degradation, but in case of PGNPNF the rate of degradation was relatively controlled due to the presence of nanoparticles [51] which might have resulted in the of bioactive composite formation of nanoparticles and PCL-Gelatin [52].

3.5. Superoxide dismutase (SOD) enzyme mimetic activity measurement

Superoxide dismutase is a naturally occurring enzyme which neutralises the superoxide anions (O_2^-) that are the primary ROS

generated in the body [53]. This antioxidant defence is essential for cell survival. CeNPs show a catalytic activity analogous to the naturally occurring SOD by alternating between two oxidation states: 3^+ and 4^+ due to an oxygen vacancy/defect in its crystal structure [19,54,55]. The presumed catalytic mechanism by which CeNPs scavenge superoxide radicals is as follows [56]:



To study the release and SOD like activity of PGNPNF in different buffer i.e. Tris and PBS buffer, we have incubated PGNPNF in these buffers for different time period (30 min, 24, 48 and 96 h) Fig. 5(a,b,c and d) followed by SOD activity measurement. Result depicts that PGNPNF suspended in Tris buffer retain their SOD activity same as CeNPs suspended in water up to 24 h Fig. 5(a and b),

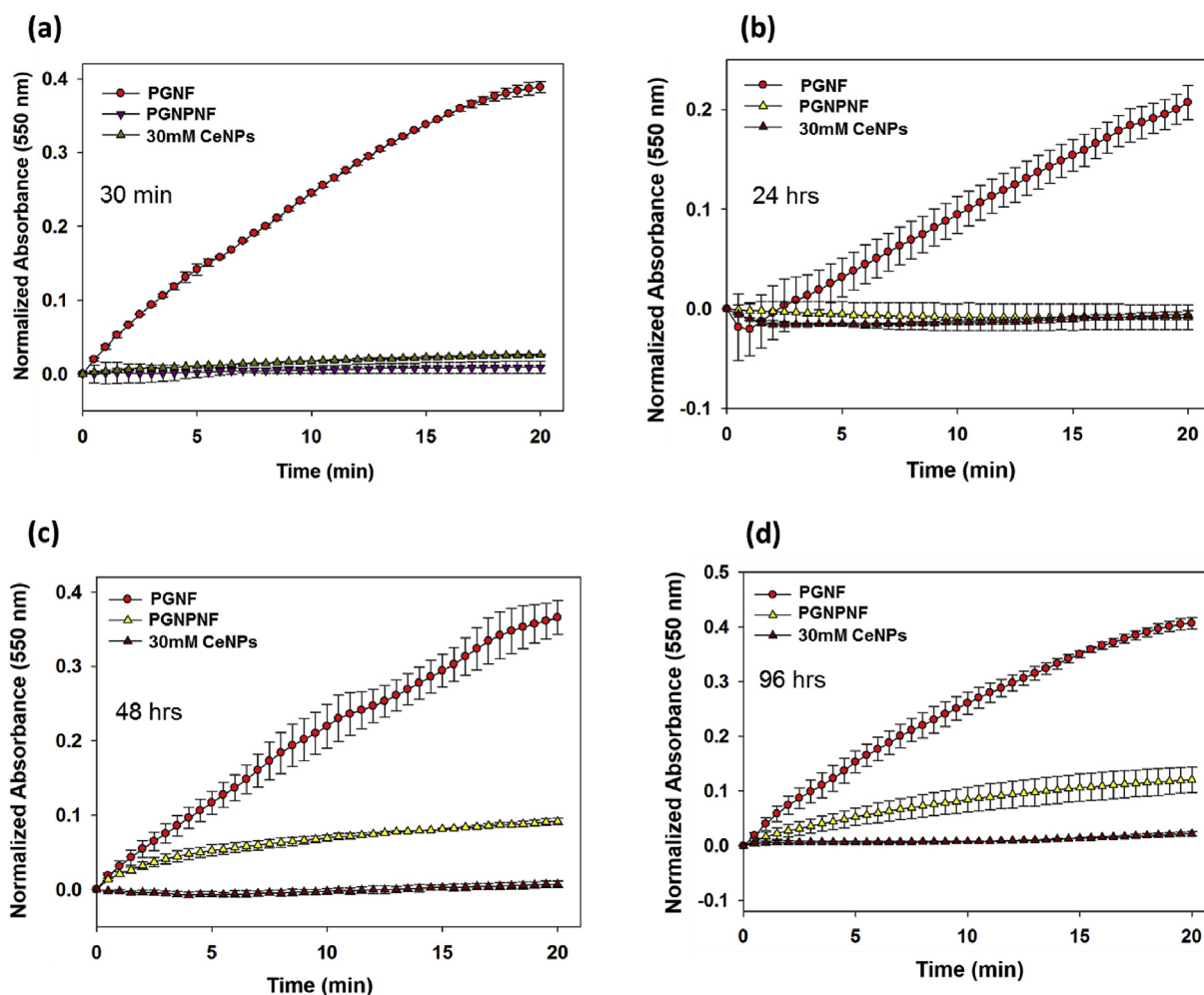


Fig. 5. SOD mimetic activity of CeNP in Tris after (a) 30 min (b) 24 h (b) (c) 48 h and (d) 96 h as measured by spectrophotometrically.

whereas, slight decrease in activity was seen at 48 and 96 h Fig. 5(c and d). Interestingly, CeNPs suspended in PBS showed less SOD activity even at 30 min and 24 h Fig. 6(a and b), it under goes complete activity loss at 48 and 96 h Fig. 6(c and d). It was previously reported by Singh et al. that phosphate shows interaction with CeNPs to form cerium phosphate, which drops its SOD activity [57]. Therefore, in our study similar results were obtained, CeNPs released in PBS buffer shows interaction with phosphate probably to form cerium phosphate which leads to altered SOD activity whereas, in Tris buffer no such interaction occurred and particles retain its activity. This study demonstrated that encapsulation of nanoparticles into nanofiber does not reduce its scavenging activity significantly. Moreover it shows the sustained release of biological active Ce nanoparticles for 96 h. As claimed the immediate release of nanoparticle would be desirable to counter the excess ROS generation in the beginning of wound healing procedure. The immobilization of Ce nanoparticles and their sustained delivery at the site of injury or regeneration by porous nanofibrous mesh can be explored for wound dressing material to skin tissue regeneration.

3.6. Cell proliferation assay

The cell viability and proliferation of 3T3-L1 cells on PGNPf and PGNF over a period of 3 days was studied by alamar blue assay

(see Fig. 7). It was observed that cells were viable and proliferating on both the samples however, the rate of cell proliferation was ~17% higher on the PGNPf compared to PGNF after 24 h (see Fig. 8). The higher cell proliferation on PGNPf continued till 72 h where ~45% more cell proliferation was observed. Furthermore, ~48% more cell growth was observed on PGNPf after 72 h compared to PGNPf at 24 h however, only ~18% growth was observed on PGNF till 72 h. The steady increase in cell proliferation on PGNPf can be attributed to the incorporated CeNPs that would have released in the culture medium. Previous studies have shown that CeNPs were able to improve cell survival by decreasing the intracellular levels of ROS produced as a result of metabolic activities, which otherwise causes cellular damage [14,20].

3.7. In vitro antioxidant study (indirect method)

In order to explore whether the CeNPs released from PGNPf were effective in scavenging ROS, a DCFDA fluorogenic probe based assay was carried out. The 3T3-L1 cells were treated with H_2O_2 in order to generate ROS. Afterwards the cells were incubated with the extracts of PGNF, PGNPf or Tris buffer (–ve control). As shown in Fig. 9, there is ~12% decrease in fluorescence intensity of DCF observed for cells treated with PGNF extract compared to negative control and a much more significant (~30%) decrease in the DCF intensity for cells treated with PGNPf extract. The decrease in the

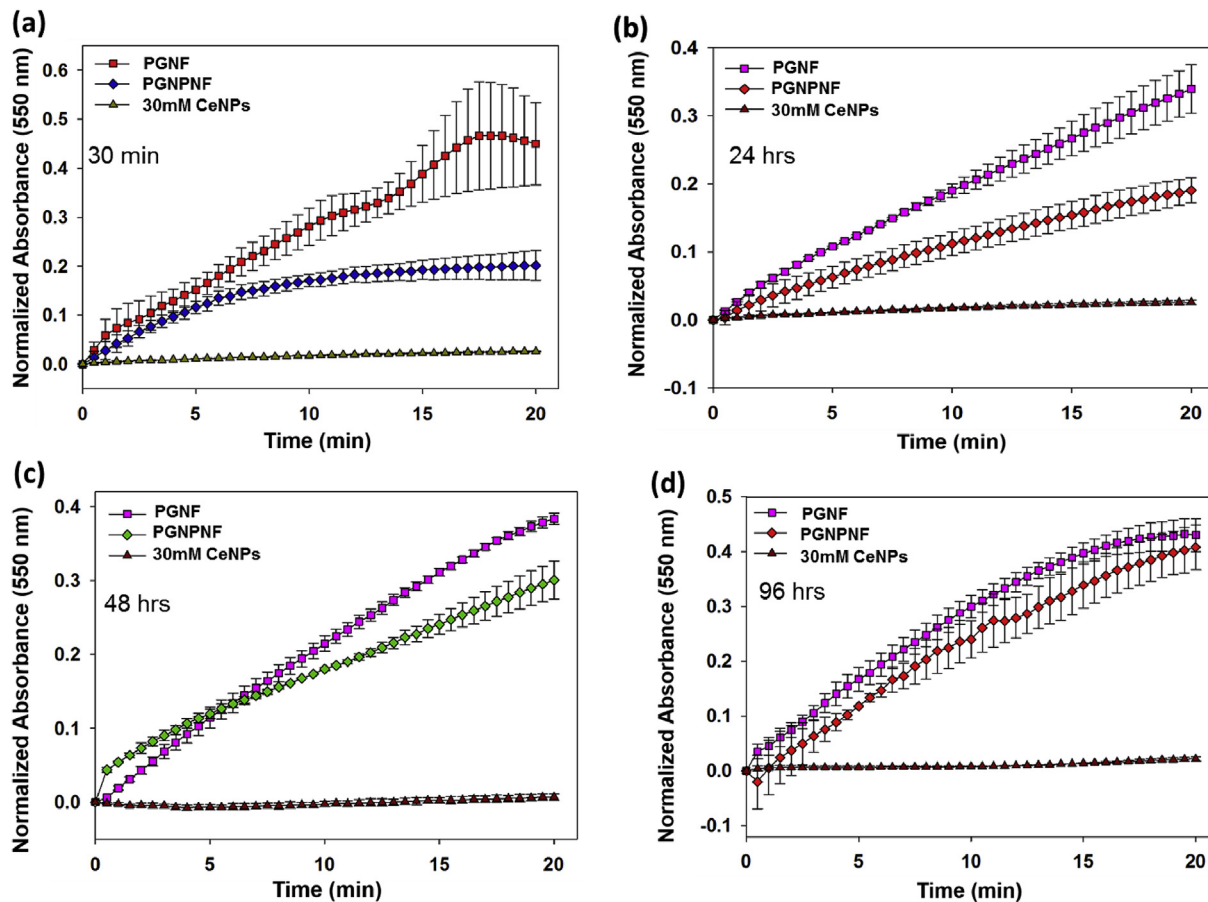


Fig. 6. SOD mimetic activity of CeNP in PBS after (a) 30 min (b) 24 h (c) 48 h and (d) 96 h as measured by spectrophotometrically.

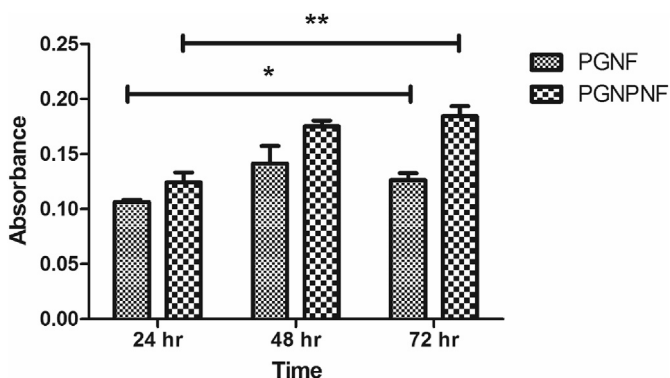


Fig. 7. 3T3 L1 cell viability and proliferation study on PGNF and PGNPNF after 24, 48 and 72 h as measured by alamar blue assay.

fluorescent activity indicates a ROS scavenging potential of the extract. The PGNF extract might contain gelatin and peptides due to partial degradation of gelatin which have a potential of scavenging ROS [58,59]. The extract of PGNPNF nanofibers is more efficient in scavenging ROS since it also contains CeNPs which are known potent ROS scavengers [20].

3.8. Intracellular ROS measurement

In corroboration with the anti-oxidant study of nanofibers, fluorescence microscopy was performed to quantify the ROS

scavenging activity of the extract. The results depict the reduced levels of fluorescence as a function of corrected total cell fluorescence, which was calculated by ImageJ software. As shown in Fig. 10, the fluorescence has reduced by 77% and 71% in the PGNPNF extract treatments collected at 30 min and 24 h respectively compared to control. However, no significant decrease was observed in the PGNF extract treatments. This signifies the role of PGNPNF to scavenge the ROS.

3.9. Cellular protection against ROS

In corroboration with cell proliferation assay and *In vitro* anti-oxidant study, the cell viability was observed to be increased significantly on PGNPNF after 24 h of H_2O_2 treatment compared to the control Fig. 11. The ~3 fold increase in the cell viability could be because of the antioxidant and ROS scavenging activity of the PGNPNF. However, the growth was not significant on PGNF (~1.2 fold increase) compared to the control. The build-up of ROS causes oxidative damage to cellular components and creates adverse effect on cell growth [60]. Less cell viability on PGNF indicates the build-up of oxidative damage because of their inadequate ROS scavenging nature when compared to control. However, ROS inhibitors enhance the cell viability and proliferation by reducing the oxidative damage [61]. Therefore, increased viability of cells on PGNPNF can be correlated to their antioxidative and ROS scavenging activity.

4. Conclusion

Elevated level of ROS at the wound site results in impaired

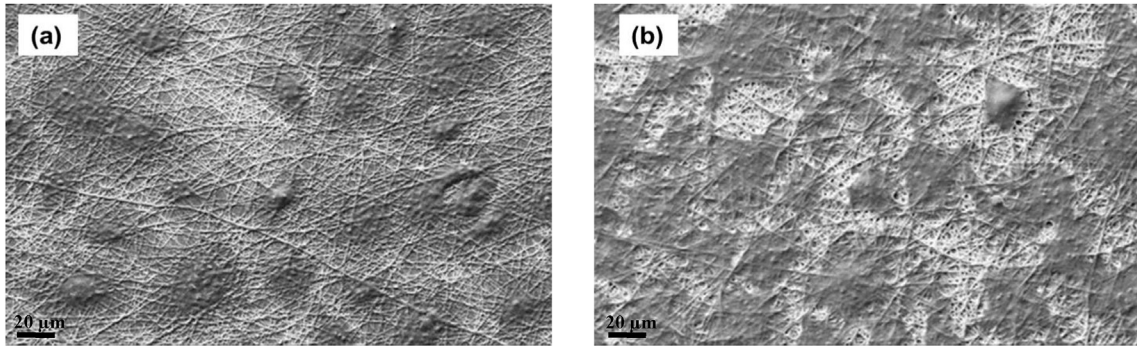


Fig. 8. SEM micrographs of 3T3 L1 fibroblast cells grown for 24 h on (a) PGNF and (b) PGNPNF.

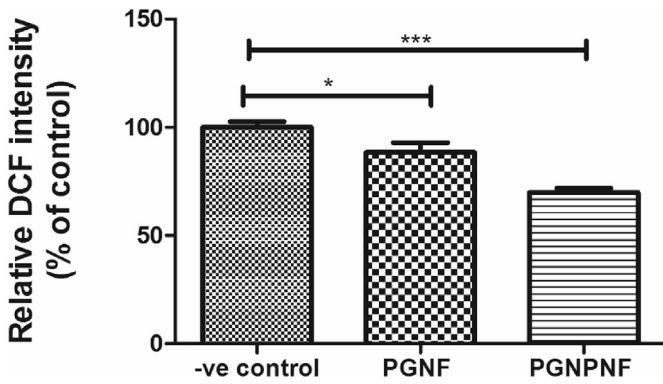


Fig. 9. ROS level measurement in 3T3-L1 by DCF fluorescence intensity.

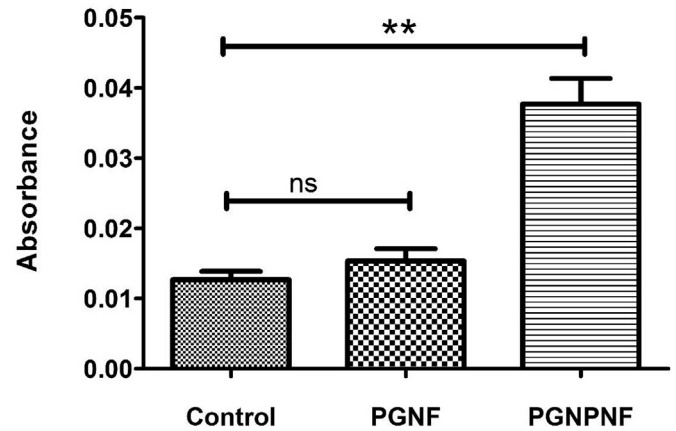


Fig. 11. 3T3 L1 cell viability against the ROS measurement by alamar blue assay.

wound healing. Therefore, nanoparticles possessing antioxidant activity have been explored for the wound healing applications. CeNPs are well known for their antioxidant properties because of their ROS scavenging activity. Hence, they protect the cells from oxidative damage by actively scavenging the ROS. In this study, ECM mimicking nanofibers loaded with CeNPs were electrospun and studied for release and SOD mimetic activity. The significant reduction in PCL crystallinity due to gelatine blending influences

degradation behaviour of scaffold. The dissolution of uncross-linked gelatine ensured the immediate release of nanoparticles as shown in SOD mimetic studies, whereas PCL ensured the structural integrity of nanofibers. Furthermore, SOD mimetic activity shows the antioxidant effect of PGNPNF in different buffer systems. Because of its antioxidant potential, enhanced cell growth on

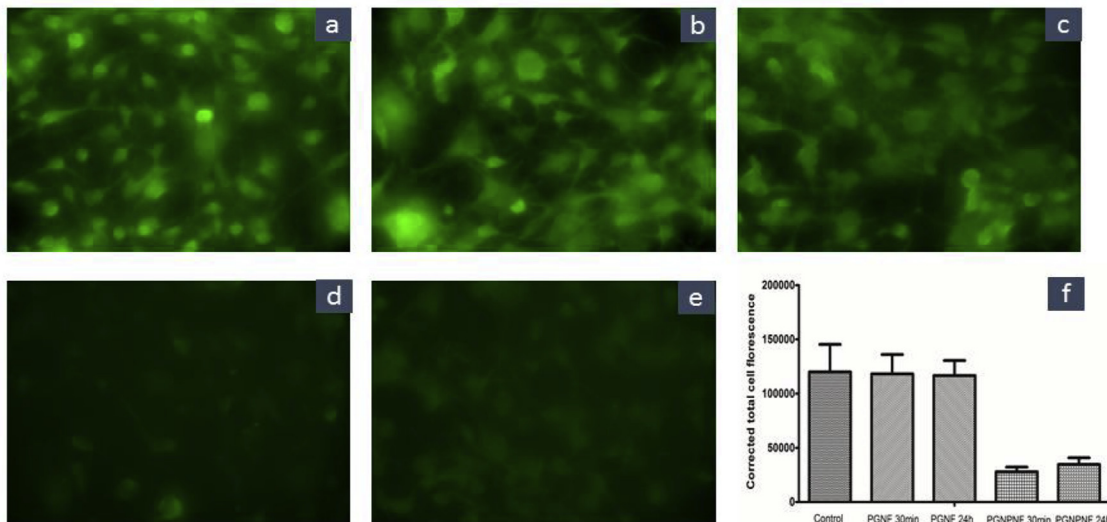


Fig. 10. Fluorescence microscopy images of (a) control (b) PGNF 30 min (c) PGNF 24 h (d) PGNPNF 30 min (e) PGNPNF 24 h and (f) corrected total cell fluorescence of respective groups.

PGNPNF was observed by alamar blue assay and SEM, which was corroborated with the ROS scavenging activity of PGNPNF. Furthermore, cyto-protection of 3T3-L1 cells from the oxidative damage of H₂O₂ also confirms the antioxidant and cell protection activity of PGNPNF. Therefore, PGNPNF meshes can be explored as wound dressing material for their antioxidant potential.

Acknowledgements

RV would like acknowledge GSBTM, Govt. of Gujarat (Grant no. GSBTM/MD/Projects/SSA/1431/2014-15) and SERB, Department of Science & Technology (DST), Govt. of India (Grant no. SB/YS/LS-13/2014) for partial financial support. HR and RS acknowledges the University Grants Commission, India and DST INSPIRE research fellowship. The authors also acknowledge the NIPER, Ahmedabad for fluorescence microscopy and IIT Gandhinagar for providing XRD facility.

References

- [1] R. Goldman, Growth factors and chronic wound healing: past, present, and future, *Adv. Skin. Wound Care* 17 (2004) 24–35.
- [2] C.N. Paiva, M.T. Bozza, Are reactive oxygen species always detrimental to pathogens? *Antioxid. Redox Signal* 20 (2014) 1000–1037.
- [3] C.K. Sen, S. Khanna, B.M. Babior, T.K. Hunt, E.C. Ellison, S. Roy, Oxidant-induced vascular endothelial growth factor expression in human keratinocytes and cutaneous wound healing, *J. Biol. Chem.* 277 (2002) 33284–33290.
- [4] S. Roy, S. Khanna, K. Nallu, T.K. Hunt, C.K. Sen, Dermal wound healing is subject to redox control, *Mol. Ther.* 13 (2006) 211–220.
- [5] C. Marchese, V. Maresca, G. Cardinali, F. Belleudi, S. Ceccarelli, M. Bellocchi, L. Frati, M.R. Torrisi, M. Picardo, UVB-induced activation and internalization of keratinocyte growth factor receptor, *Oncogene* 22 (2003) 2422–2431.
- [6] T. Goldkorn, N. Balaban, K. Matsukuma, V. Chea, R. Gould, J. Last, C. Chan, C. Chavez, EGF-Receptor phosphorylation and signaling are targeted by H2O2 redox stress, *Am. J. Respir. Cell Mol. Biol.* 19 (1998) 786–798.
- [7] W. Droge, Free radicals in the physiological control of cell function, *Physiol. Rev.* 82 (2002) 47–95.
- [8] S. Dhali, D. Do, M. Garcia, D.S. Wijesinghe, A. Brandon, J. Kim, A. Sanchez, J. Lyubovitsky, S. Gallagher, E.A. Nothnagel, C.E. Chalfant, R.P. Patel, N. Schiller, M. Martins-Green, A novel model of chronic wounds: importance of redox imbalance and biofilm-forming bacteria for establishment of chronicity, *PLoS One* 9 (2014), e109848.
- [9] V.W. Wong, G.C. Gurtner, Tissue engineering for the management of chronic wounds: current concepts and future perspectives, *Exp. Dermatol* 21 (2012) 729–734.
- [10] P.G. Rodriguez, F.N. Felix, D.T. Woodley, E.K. Shim, The role of oxygen in wound healing: a review of the literature, *Dermatol. Surg.* 34 (2008) 1159–1169.
- [11] H.M. Shen, S. Pervaiz, Reactive oxygen species in cell fate decisions, in: Z. Dong, X.-M. Yin (Eds.), *Essentials of Apoptosis: a Guide for Basic and Clinical Research*, Humana Press, Totowa, NJ, 2009, pp. 199–221.
- [12] J.V. Dovi, A.M. Szpaderska, L.A. DiPietro, Neutrophil function in the healing wound: adding insult to injury? *Thromb. Haemost.* 92 (2004) 275–280.
- [13] S.M. McCarty, C.A. Cochrane, P.D. Clegg, S.L. Percival, The role of endogenous and exogenous enzymes in chronic wounds: a focus on the implications of aberrant levels of both host and bacterial proteases in wound healing, *Wound Repair Regen.* 20 (2012) 125–136.
- [14] S. Chigurupati, M.R. Mughal, E. Okun, S. Das, A. Kumar, M. McCaffery, S. Seal, M.P. Mattson, Effects of cerium oxide nanoparticles on the growth of keratinocytes, fibroblasts and vascular endothelial cells in cutaneous wound healing, *Biomaterials* 34 (2013) 2194–2201.
- [15] R. Davan, R. Prasad, V.S. Jukka, R. Aparna, A. Phani, B. Jacob, P.C. Salins, D. Raju, Cerium oxide nanoparticles promotes wound healing activity in in-vivo animal model, *J. Bionanosci.* 6 (2012) 78–83.
- [16] S. BarathManiKanth, K. Kalishwaralal, M. Sriram, S.R.K. Pandian, H.-S. Yoon, S. Eom, S. Gurunathan, Anti-oxidant effect of gold nanoparticles restrains hyperglycemic conditions in diabetic mice, *J. Nanobiotechnol.* 8 (2010) 16.
- [17] H. Wei, E. Wang, Nanomaterials with enzyme-like characteristics (nanozymes): next-generation artificial enzymes, *Chem. Soc. Rev.* 42 (2013) 6060–6093.
- [18] A.S. Karakoti, S. Singh, A. Kumar, M. Malinska, S.V. Kuchibhatla, K. Wozniak, W.T. Self, S. Seal, PEGylated nanoceria as radical scavenger with tunable redox chemistry, *J. Am. Chem. Soc.* 131 (2009) 14144–14145.
- [19] C. Korsvik, S. Patil, S. Seal, W.T. Self, Superoxide dismutase mimetic properties exhibited by vacancy engineered ceria nanoparticles, *Chem. Commun.* 14 (2007) 1056–1058.
- [20] R. Singh, A.S. Karakoti, W. Self, S. Seal, S. Singh, Redox-sensitive cerium oxide nanoparticles protect human keratinocytes from oxidative stress induced by glutathione depletion, *Langmuir* 32 (2016) 12202–12211.
- [21] I. Celardo, E. Traversa, L. Ghibelli, Cerium oxide nanoparticles: a promise for applications in therapy, *J. Exp. Ther. Oncol.* 9 (2011) 47–51.
- [22] C. Xu, X. Qu, Cerium oxide nanoparticle: a remarkably versatile rare earth nanomaterial for biological applications, *NPG Asia Mater* 6 (2014) e90.
- [23] E.J. Chong, T.T. Phan, I.J. Lim, Y.Z. Zhang, B.H. Bay, S. Ramakrishna, C.T. Lim, Evaluation of electrospun PCL/gelatin nanofibrous scaffold for wound healing and layered dermal reconstitution, *Acta Biomater.* 3 (2007) 321–330.
- [24] G. Jin, Y. Li, M.P. Prabhakaran, W. Tian, S. Ramakrishna, In vitro and in vivo evaluation of the wound healing capability of electrospun gelatin/PLLCL nanofibers, *J. Bioact. Compat. Polym.* 29 (2014) 628–645.
- [25] M. Begloul, A. Haghi, Electrospun biodegradable and biocompatible natural nanofibers: a detailed review, *Cellul. Chem. Technol.* 42 (2008) 441.
- [26] S.J. Liu, Y.C. Kau, C.Y. Chou, J.K. Chen, R.C. Wu, W.L. Yeh, Electrospun PLGA/collagen nanofibrous membrane as early-stage wound dressing, *J. Membr. Sci.* 355 (2010) 53–59.
- [27] D. Jhala, H. Rather, R. Vasita, Polycaprolactone-chitosan nanofibers influence cell morphology to induce early osteogenic differentiation, *Biomater. Sci.* 4 (2016) 1584–1595.
- [28] R. Yao, J. He, G. Meng, B. Jiang, F. Wu, Electrospun PCL/Gelatin composite fibrous scaffolds: mechanical properties and cellular responses, *J. Biomater. Sci. Polym. Ed.* 27 (2016) 824–838.
- [29] R. Goyal, L.K. Macri, H.M. Kaplan, J. Kohn, Nanoparticles and nanofibers for topical drug delivery, *J. Control. Release* 240 (2016) 77–92.
- [30] R.S. Tigli, N.M. Kazaroglu, B. Mavis, M. Gumusderelioglu, Cellular behavior on epidermal growth factor (EGF)-immobilized PCL/gelatin nanofibrous scaffolds, *J. Biomater. Sci. Polym. Ed.* 22 (2011) 207–223.
- [31] A. GhavamiNejad, A. Rajan Unnithan, A. Ramachandra Kurup Sasikala, M. Samarikhajaj, R.G. Thomas, Y.Y. Jeong, N. Nasserri, P. Murugesan, D. Wu, C. Hee Park, C.S. Kim, Mussel-inspired electrospun nanofibers functionalized with size-controlled silver nanoparticles for wound dressing application, *ACS Appl. Mater. Interfaces* 7 (2015) 12176–12183.
- [32] M. Al-Omair, Synthesis of antibacterial silver–poly(ϵ -caprolactone)-methacrylic acid graft copolymer nanofibers and their evaluation as potential wound dressing, *Polymers* 7 (2015) 1464.
- [33] R.H. Dong, Y.X. Jia, C.-C. Qin, L. Zhan, X. Yan, L. Cui, Y. Zhou, X. Jiang, Y.-Z. Long, In situ deposition of a personalized nanofibrous dressing via a handy electrospinning device for skin wound care, *Nanoscale* 8 (2016) 3482–3488.
- [34] D.N. Heo, D.H. Yang, J.B. Lee, M.S. Bae, J.H. Kim, S.H. Moon, H.J. Chun, C.H. Kim, H.N. Lim, I.K. Kwon, Burn-wound healing effect of gelatin/polyurethane nanofiber scaffold containing silver-sulfadiazine, *J. Biomed. Nanotechnol.* 9 (2013) 511–515.
- [35] M.A. Oraby, A.I. Waley, A.I. El-Dewany, E.A. Saad, B. Abd El-Hady, Electrospinning of gelatin functionalized with silver nanoparticles for nanofiber fabrication, *Model Numer. Simul. Mater Sci.* 3 (2013) 95–105.
- [36] S.M. Jung, G.H. Yoon, H.C. Lee, H.S. Shin, Chitosan nanoparticle/PCL nanofiber composite for wound dressing and drug delivery, *J. Biomater. Sci. Polym. Ed.* 26 (2015) 252–263.
- [37] D. Jung, I. Minami, S. Patel, J. Lee, B. Jiang, Q. Yuan, L. Li, S. Kobayashi, Y. Chen, K.-B. Lee, N. Nakatsuji, Incorporation of functionalized gold nanoparticles into nanofibers for enhanced attachment and differentiation of mammalian cells, *J. Nanobiotechnol.* 10 (2012), 23–23.
- [38] J.E. Kim, J. Lee, M. Jang, M.H. Kwak, J. Go, E.K. Kho, S.H. Song, J.E. Sung, J. Lee, D.Y. Hwang, Accelerated healing of cutaneous wounds using phytochemically stabilized gold nanoparticle deposited hydrocolloid membranes, *Biomater. Sci.* 3 (2015) 509–519.
- [39] O. Akturk, K. Kismet, A.C. Yasti, S. Kuru, M.E. Duymus, F. Kaya, M. Caydere, S. Hucumenoglu, D. Keskin, Collagen/gold nanoparticle nanocomposites: a potential skin wound healing biomaterial, *J. Biomater. Appl.* 31 (2016) 283–301.
- [40] S.M. Jung, S.K. Min, H.C. Lee, Y.S. Kwon, M.H. Jung, H.S. Shin, Spirulina-PCL nanofiber wound dressing to improve cutaneous wound healing by enhancing antioxidative mechanism, *J. Nanomater* 2016 (2016) 10.
- [41] A.S. Karakoti, S. Singh, A. Kumar, M. Malinska, S.V.N.T. Kuchibhatla, K. Wozniak, W.T. Self, S. Seal, PEGylated nanoceria as radical scavenger with tunable redox chemistry, *J. Am. Chem. Soc.* 131 (2009) 14144–14145.
- [42] H. Jin, N. Wang, L. Xu, S. Hou, Synthesis and conductivity of cerium oxide nanoparticles, *Mater. Lett.* 64 (2010) 1254–1256.
- [43] S. Gautam, C.-F. Chou, A.K. Dinda, P.D. Potdar, N.C. Mishra, Surface modification of nanofibrous polycaprolactone/gelatin composite scaffold by collagen type I grafting for skin tissue engineering, *Mater Sci. Eng. C Mater Biol. Appl.* 34 (2014) 402–409.
- [44] L.H. Chong, M.M. Lim, N. Sultana, Fabrication and evaluation of polycaprolactone/gelatin-based electrospun nanofibers with antibacterial properties, *J. Nanomater* 2015 (2015) 15.
- [45] X. Yang, J. Yang, L. Wang, B. Ran, Y. Jia, L. Zhang, G. Yang, H. Shao, X. Jiang, Pharmaceutical intermediate-modified gold nanoparticles: against multidrug-resistant bacteria and wound-healing application via electrospun scaffold, *ACS Nano* 11 (2017) 5737–5745.
- [46] P. Denis, J. Dulnik, P. Sajkiewicz, Electrospinning and structure of biocomponent polycaprolactone/gelatin nanofibers obtained using alternative solvent system, *Int. J. Polym. Mater* PO 64 (2015) 354–364.
- [47] V. Sencadas, C. Ribeiro, J. Nunes-Pereira, V. Correia, S. Lanceros-Méndez, Fiber average size and distribution dependence on the electrospinning parameters of poly(vinylidene fluoride–trifluoroethylene) membranes for biomedical applications, *Appl. Phys. A* 109 (2012) 685–691.

- [48] S. Gautam, A.K. Dinda, N.C. Mishra, Fabrication and characterization of PCL/gelatin composite nanofibrous scaffold for tissue engineering applications by electrospinning method, *Mater. Sci. Eng. C Mater. Biol. Appl.* 33 (2013) 1228–1235.
- [49] K. Ghosal, S. Thomas, N. Kalarikkal, A. Gnanamani, Collagen coated electrospun polycaprolactone (PCL) with titanium dioxide (TiO₂) from an environmentally benign solvent: preliminary physico-chemical studies for skin substitute, *J. Polym.* 21 (2014) 410.
- [50] M.P. Bajgai, K.-W. Kim, D. Chandra Parajuli, Y.C. Yoo, W.D. Kim, M.-S. Khil, H.Y. Kim, In vitro hydrolytic degradation of poly(ϵ -caprolactone) grafted dextran fibers and films, *Polym. Degrad. Stab.* 93 (2008) 2172–2179.
- [51] D. Wang, L. Xuan, H. Zhong, Y. Gong, X. Shi, F. Ye, Y. Li, Q. Jiang, Incorporation of well-dispersed calcium phosphate nanoparticles into PLGA electrospun nanofibers to enhance the osteogenic induction potential, *RSC Adv.* 7 (2017) 23982–23993.
- [52] J. Huang, J. Xiong, J. Liu, W. Zhu, D. Wang, Investigation of the in vitro degradation of a novel polylactide/nanohydroxyapatite composite for artificial bone, *J. Nanomater.* 2013 (2013) 10.
- [53] J.M. McCord, I. Fridovich, Superoxide dismutase: an enzymic function for erythrocyte hemocuprein, *J. Biol. Chem.* 244 (1969) 6049–6055.
- [54] E. Heckert, A. Karakoti, S. Seal, W.T. Self, The role of cerium redox state in the SOD mimetic activity of nanoceria, *Biomaterials* 29 (2008) 2705–2709.
- [55] Y. Li, X. He, J.J. Yin, Y. Ma, P. Zhang, J. Li, Y. Ding, J. Zhang, Y. Zhao, Z. Chai, Z. Zhang, Acquired superoxide-scavenging ability of ceria nanoparticles, *Angew. Chem. Int. Ed. Engl.* 54 (2015) 1832–1835.
- [56] B.C. Nelson, M.E. Johnson, M.L. Walker, K.R. Riley, C.M. Sims, Antioxidant cerium oxide nanoparticles in biology and medicine, *Antioxidants* 5 (2016) 15.
- [57] S. Singh, T. Dosani, A. Karakoti, A. Kumar, S. Seal, W.T. Self, A phosphate-dependent shift in redox state of cerium oxide nanoparticles and its effects on catalytic properties, *Biomaterials* 32 (2011) 6745–6753.
- [58] Y. Zhuang, L. Sun, Preparation of reactive oxygen scavenging peptides from tilapia (*Oreochromis niloticus*) skin gelatin: optimization using response surface methodology, *J. Food Sci.* 76 (2011) C483–C489.
- [59] S.W. Himaya, B. Ryu, D.H. Ngo, S.K. Kim, Peptide isolated from Japanese flounder skin gelatin protects against cellular oxidative damage, *J. Agric. Food Chem.* 60 (2012) 9112–9119.
- [60] J.S. Valentine, D.L. Wertz, T.J. Lyons, L.-L. Liou, J.J. Goto, E.B. Gralla, The dark side of dioxygen biochemistry, *Curr. Opin. Chem. Biol.* 2 (1998) 253–262.
- [61] Q. Huang, B. Gao, Q. Jie, B.Y. Wei, J. Fan, H.Y. Zhang, J.K. Zhang, X.J. Li, J. Shi, Z.J. Luo, L. Yang, J. Liu, Ginsenoside-Rb2 displays anti-osteoporosis effects through reducing oxidative damage and bone-resorbing cytokines during osteogenesis, *Bone* 66 (2014) 306–314.